



Sucrose-mediated formation and adhesion strength of *Streptococcus mutans* biofilms on titanium

Laura J. Waldman^{a,1}, Tony Butera^{a,1}, James D. Boyd^b, Martha E. Grady^{a,*}

^a Department of Mechanical and Aerospace Engineering University of Kentucky, Lexington, KY, 40506, USA

^b Department of Mechanical Engineering Clemson University, Clemson, SC, 29634, USA

ARTICLE INFO

Keywords:

Biofilms
Laser spallation
Scanning electron microscopy
Adhesion
Dental implants
Streptococcus mutans
Sucrose
Titanium

ABSTRACT

Biofilms consist of bacterial cells surrounded by a matrix of extracellular polymeric substance (EPS), which protects the colony from many countermeasures, including antibiotic treatments. Growth and formation of bacterial biofilms are affected by nutrients available in the environment. In the oral cavity, the presence of sucrose affects the growth of *Streptococcus mutans* that produce acids that erode enamel and form dental caries. Biofilm formation on dental implants commonly leads to severe infections and can restrict osseointegration necessary for the implant to be successful. This work determines the effect of sucrose concentration on biofilm EPS formation and adhesion of *Streptococcus mutans*, a common oral colonizer, to titanium substrates simulating common dental implants. Biofilm formation and profiles are visualized at high magnification with scanning electron microscopy (SEM). Large mounds and complex structures consisting of bacterial cells and EPS can be seen in biofilms at sucrose concentrations that are favorable for biofilm growth. The laser spallation technique is used to apply stress wave loading to the biofilm, causing the biofilm to delaminate at a critical tensile stress threshold. The critical tensile stress threshold is the adhesion strength. Because laser spallation applies the stress loading to the rear of the substrate, bulk adhesion properties of the biofilm can be determined despite the heterogeneous composition and low cohesion strength of the biofilm. Statistical analysis reveals that adhesion strength of biofilms initially increase with increasing sucrose concentration and then decrease as sucrose concentration continues to increase. The adhesion strength of bacterial biofilms to the substrate in this study is compared to the adhesion of osteoblast-like cells to the same substrates published previously. When sucrose is present in the biofilm growth environment, *S. mutans* adhesion is higher than that of the osteoblast-like cells. Results of this study suggest sucrose-mediated *S. mutans* biofilms may outcompete osteoblasts in terms of adhesion during osseointegration, which could explain higher rates of peri-implant disease associated with high sugar diets. Further studies demonstrating adhesion differentials between biofilms and cells including co-cultures are needed and motivated by the present work.

1. Introduction

Bacterial infections are a recurring concern for permanent structural implants such as hip and dental implants, as well as temporary implants such as urinary tract devices [1]. For dental implants, the success of the procedure relies on the osseointegration of the implant into existing bone. Osseointegration occurs when bone tissue grows around an implant and comes into direct contact with the implant material [2]. However, the growth of bacterial biofilms on implant surfaces can prevent osseointegration and lead to failure of the implant [3,4].

Bacterial biofilms consist of cells surrounded by extracellular polymeric substance (EPS) that protects the colony from treatment strategies such as antibiotics or mechanical removal [5–7]. The EPS matrix contributes to the cohesion between individual bacterial cells, as well as adhesion of the biofilm to the substrate surface [8]. Additionally, biofilm growth is affected by specific environmental factors in the growth area, including substrate material, surface roughness, hydrophobicity, and hydrodynamic pressure and temperature, as well as the concentration of nutrients such as sucrose, glucose, and other carbohydrates [9–15]. Nutrient availability in particular has been shown to affect properties of

* Corresponding author.

E-mail address: m.grady@uky.edu (M.E. Grady).

¹ Equal Contribution.

the biofilm such as genetic expression in EPS [16], quantity or thickness of the biofilm [17], or the adhesion of the biofilm to a substrate [18].

Streptococcus mutans is a common oral colonizer that causes dental caries [19] and is often found in the multispecies biofilms that grow on dental implants and can contribute to long term health issues surrounding implants [20–22]. Sucrose, a nutrient which has been demonstrated to support the growth of *S. mutans* biofilms, is often present in the oral cavity due to sucrose concentrations in commercial foods [23]. Previous studies provided information on the relationship between sucrose and the constituents of the biofilm [19,24]; however, the effect of the sucrose concentration on the adhesion of the biofilm to a dental implant surface and how this adhesion might affect the osseointegration of the implant is not yet experimentally determined.

Biofilm adhesion characterization is challenging due to the complexity of the material. Because biofilms are heterogeneous and exhibit low cohesive strength, many of the methods used for thin film adhesion, such as pull tests, are incompatible with biofilms [10]. Some methods examine the interactions between a single bacterial cell and the surface using atomic force microscopy, but these techniques are not applicable to macroscale adhesion of the bulk biofilm [25] because atomic force microscopy extracts peak pull off forces that result in microscale adhesion on the order of single nN without known contact areas [26]. Hydrodynamic flow and jet impingement techniques can provide information about adhesion of biofilms by determining the shear stress necessary to remove a biofilm from a surface. However, shear flow on the biofilm surface can lead to the formation of ripple patterns or changes in biofilm velocity [27] and the low cohesion of biofilms can lead to erroneous measurements if the shear stress causes the biofilm to separate, rather than detach from the substrate [28]. Other methods for quantifying biofilm formation examine cell presence or EPS presence within the biofilm but do not provide force-based information on the interaction between the biofilm and the substrate surface [29].

The laser spallation technique is a quantitative adhesion strength measurement method that applies stress wave loading, causing separation of a film of interest from the substrate at a critical stress value [18, 30,31]. Because the stress load is applied indirectly to the material interface through impingement of a pulsed laser on the back side of the specimen, laser spallation is valuable for characterizing bulk adhesion properties of a wide range of materials. Material interfaces as diverse as gels [32], laminated composites [33], thin metal films [34,35], polymer films [36], and mammalian cells on substrates [37] have been investigated using the laser spallation technique. The shock loading conditions are also used to quantify dynamic behaviors of materials [38,39] and in the development of stress-reporting materials [40]. The laser spallation technique is advantageous for studying the adhesion of biological materials including bacterial biofilms where the cohesiveness of the film is low relative to the adhesion of the film to the substrate and adhesion is measured over mm² of area accounting for lower coverage on a small scale. Previous studies on biological samples including bacterial biofilms [18] and osteoblasts [41] have investigated the adhesion of these cells to simulated dental implants. However, these studies fail to address how these cells may respond to changes in the nutrient concentration in the environment, or how these species may compete with each other in the same environment.

This work examines the effects of sucrose concentration on *S. mutans* biofilm structure and formation as well as biofilm adhesion to a titanium substrate similar to those used in dental implants. Preserved biofilm structures are imaged with electron microscopy to identify changes in biofilm morphology due to increased sucrose concentration. Electron microscopy combined with the best-known EPS preservation technique provides the high resolution needed to visualize both individual cells and EPS structures within the biofilms [29,42]. The laser spallation technique is used to quantitatively determine the effect of sucrose concentration on the adhesion strength of the biofilm to the titanium substrate. Confidence intervals for the failure stress of bacterial biofilms are

determined with Weibull modeling.

2. Experimental

2.1. Bacterial culture & biofilm preparation

Streptococcus mutans (Wild type Xc) [43] suspended in Todd Hewitt Yeast broth (THY, VWR) with 20% glycerol is kept as frozen stock in a –80 °C freezer. Frozen bacteria stock is thawed gently using a warming bath at 37 °C. A 15 mL centrifuge tube was filled with 5 mL of THY and inoculated with 1 µL of bacteria stock. The inoculated centrifuge tube is placed into a warming bath at 37 °C and cultured for 24 h. At 24 h, the culture is in the stationary growth phase. After this period, the optical density (OD) at 600 nm is measured using a GENESYS™ 30 Visible Spectrophotometer (Thermo Scientific). THY is added to each centrifuge tube to adjust the optical density of the bacterial solution to 0.7. At this optical density, the corresponding CFU count is 2.2×10^8 units.

Biofilms are grown on substrate assemblies for laser spallation or glass slides commercially prepared with a 100 nm layer of titanium (Deposition Research Laboratory, Inc.) in Petri dishes for scanning electron microscopy. Titanium coated slides are smooth and have an RMS surface roughness of 8.9 ± 0.80 nm, which is very small relative to the size scale of bacterial cells. RMS Surface roughness is determined using a JPK NanoWizard 4a AFM in contact mode over 7 regions of $10 \mu\text{m} \times 10 \mu\text{m}$. Substrate assemblies and titanium coated slides are sterilized using 70% ethanol in DI water followed by UV irradiation for 30 min. Following sterilization, 1 mL of bacterial solution with OD₆₀₀ equal to 0.7 and 3 mL of THY plus sucrose (VWR) at chosen concentrations is added to each dish. Concentrations of sucrose in THY used in this study are chosen based on sucrose presence in commercial food products and are: 0 mM, 37.5 mM, 75 mM, 375 mM and 750 mM sucrose. Dishes are placed in a stationary incubator at 37 °C with 5% CO₂ and cultured for 24 h. Media is aspirated and biofilms are gently rinsed by pipetting phosphate buffered saline (PBS, VWR) into the dish upstream from the biofilm growth area to remove any detached bacteria.

2.2. Sample fixation for SEM

For electron microscopy, biofilms are grown on 25 mm wide glass slides coated with a 100 nm thick layer of titanium (DRLI) that are cut to 12 mm lengths with a diamond-tip scribe (MikroMasch) and placed inside 35 mm Petri dishes. *S. mutans* biofilms are fixed with Methacarn (Methanol – 60%, Chloroform – 30%, Acetic acid (glacial) – 10% (all VWR)) [44] for 1 h. The samples are rinsed by pipetting PBS into the dish upstream from the biofilm growth area to remove any detached bacteria followed by progressive dehydration in increasing ethanol (VWR) concentrations (30% for 15 min, 50% for 15 min, 70% for 15 min, 90% for 20 min, 100% for 20 min). Samples are dried in a Leica CPD 300 critical point dryer with a total cycle time of 4 h. Samples are sputter coated with a 5 nm layer gold/palladium with a Leica ACE 600 sputter coater in preparation for electron microscopy.

2.3. Scanning electron microscopy

Samples are imaged with a FEI Quanta 250 SEM. During top-down scanning electron microscopy, 6 biofilms prepared with each of 5 sucrose concentrations are imaged. Each of the prepared 30 biofilms is imaged at 4 distinct locations with increasing magnification and an accelerating voltage of 5 keV and working distance of 10 mm. The 5 magnifications chosen are 250x, 2500x, 5000x, 10000x, and 15000x. A total of 120 SEM images are recorded for each sucrose concentration, for a combined total of 600 top-down images in this study. The raw data required to reproduce these findings are available to download from <https://doi.org/10.18126/d1bg-nwtg> via the Materials Data Facility [45,46].

In addition to top-down imaging, biofilms are also imaged in profile

to obtain information about biofilm formation and film thickness. Substrates with dried and sputter coated biofilms are placed sideways in metal mounting springs on specimen mounts and held with copper tape. The edge of the biofilm and elevated features in the biofilm are imaged with the same scanning electron microscope conditions. Biofilm images are captured at a minimum of six locations along the 25 mm length of one substrate for each sucrose concentration. Elevated biofilm features located away from the substrate edge are imaged sequentially, by first focusing on the edge of the substrate and then changing the focus to image elevated biofilm features in increasing distance away from the substrate edge.

2.4. Adhesion testing

The laser spallation technique is used to determine the effect of sucrose concentration on bacterial biofilm adhesion. A schematic of the experimental setup used for biofilm-substrate adhesion measurements is shown in Fig. 1. A 1064 nm wavelength single pulsed Nd:YAG laser (Quanta-Ray INDI, Spectra-Physics) with a pulse duration of 10 ns and adjustable energy from 0 to 300 mJ is used to initiate film spallation. A laser pulse is focused to a 2.2 mm spot size and reflects vertically to impinge upon the substrate assembly.

The substrate assembly includes a titanium-coated glass slide adhered to a 35 mm Petri dish with a 25 mm diameter hole such that a biofilm can be cultured directly on the titanium surface. On the side opposite of biofilm growth are two layers designed to generate a stress wave of sufficient amplitude to spall the biofilm. The aluminum layer (approximately 300 nm in thickness) absorbs the infrared laser pulse and rapidly becomes a gas. Because the absorbing layer is sandwiched between the substrate and a confining layer of sodium silicate (approximately 5.5 μm in thickness), the rapid gasification of the aluminum sends a large amplitude compressive wave into the substrate and then into the biofilm. The compressive stress wave reflects at the free surface of the biofilm causing a tensile load on the biomaterial-titanium interface. When the amplitude of the tensile load is greater than the adhesive strength of the film, the film separates from the substrate. Because the stress wave loading is applied to the underside of the substrate, the failure stress reflects the bulk behavior of the biofilm. Each biofilm is loaded in this manner at multiple locations by moving the sample dish using translation stages. Loading regions are separated by a gap equal to the spot size to mitigate any effect from previous loads on current loading areas. The substrate assembly and the experimental method of spallation testing are discussed in greater detail in Boyd *et al.* [18,30].

During spallation testing, *S. mutans* biofilms are loaded over a range of fluences (7.93–79.4 mJ/mm²), which is the energy of a single pulse divided by the spot size area. Calibration experiments are performed to convert fluence values to interface stress values based on one dimensional wave propagation and transmission coefficients. Procedures for

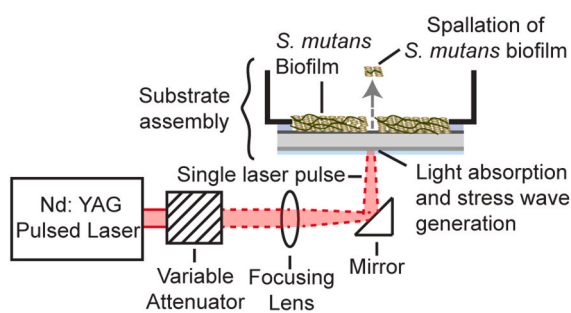


Fig. 1. Schematic of laser spallation setup used during experimentation where a single pulse from an Nd: YAG laser impinges upon a substrate assembly resulting in ejection of *S. mutans* biofilm. Figure adapted from Ref. [30].

calibration experiments can be read in further detail in previous experiments [30,31].

Spallation testing includes 12–15 loading locations per substrate assembly to determine the fluence at which failure occurs. For each sucrose concentration, 12 biofilms are tested, resulting in a total of over 100 loaded regions for this study. Failure is recorded when visible concentric ejection of the film is observed at the loaded region. The failure rate at each fluence is used as input to a Weibull failure model to determine the adhesion strength for each biofilm.

2.5. Weibull modeling of film failure

Due to the natural heterogeneity of biological materials, spallation occurs over a range of loading values. The failure statistics, $F(\sigma_{\text{int,peak}})$, are fit to a two parameter cumulative Weibull distribution function (Equation (1)) [47] to determine the adhesion strength for each sucrose concentration in this study. Weibull analysis, common in macroscopic adhesion analyses [48,49], calculates the half-life from a Weibull distribution and is used as the adhesion strength.

$$F(\sigma_{\text{int,peak}}) = 1 - e^{-\left(\frac{\sigma_{\text{int,peak}}}{\alpha}\right)^\beta} \quad (1)$$

A statistical method was developed in Boyd *et al.* [30], and improved in this paper, which considers the variability in both film failure data and calibrated interface stress. Previous statistical analysis methods have low RMS difference between the experimental film failure data and the Weibull model for *S. mutans* biofilms, resulting in asymptotic confidence intervals that were unrealistically small. Interface stress and film failure data are resampled with replacement (bootstrapped) simultaneously 1000 times to obtain simulated Weibull parameters alpha and beta. The non-linearity of the sampled beta values prevented a simple confidence interval approach. Instead, the beta values are log transformed before obtaining a 95% confidence interval, and then transformed back to the original scale. The Weibull model is interpolated for each of the 1000 simulations to obtain the interface stress that correlates to 50% failure, which represents the adhesion strength of the biofilm to the substrate. The 95% C.I. represents the range of plausible values for the median value for the adhesion strength of the biofilm to the titanium substrate.

3. Results and discussion

3.1. Optical visualization

Stable biofilms are observed for each sucrose concentration indicated by the opaque film that forms on the titanium coated substrates as shown in Fig. 2(b, c). Prior to bacteria deposition, the titanium surface of the substrate is clear and reflective (Fig. 2(a)). Biofilms grown with 0 mM sucrose have incomplete coverage of the substrates, and the titanium surface can be seen through the biofilm, as shown in Fig. 2(b). Substrates with biofilms grown with any non-zero sucrose concentration in this study, such as the 37.5 mM concentration shown in Fig. 2(c), have more consistent coverage. For these concentrations, a cloudy and continuous film covers the substrate completely. Among biofilms grown with sucrose, visual inspection reveals very little that differentiates the samples with differing concentrations of sucrose.

3.2. Top-down electron microscopy

Biofilms are imaged at high magnification with electron microscopy to compare biofilm structures for each sucrose concentration. At all concentrations, *S. mutans* cells form in chains and are surrounded by EPS, though the length of the chains and amount of EPS varies by sucrose concentration. Top-down imaging reveals differences between biofilms grown with different sucrose concentrations. Biofilm samples

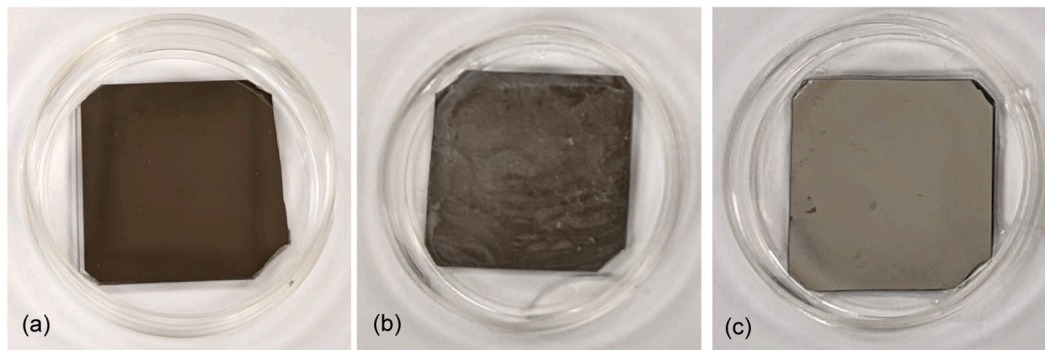


Fig. 2. Optical images of titanium coated substrates inside 35 mm Petri dishes. (a) Bare substrate (b) Substrate with *S. mutans* biofilm grown with 0 mM sucrose (c) Substrate with *S. mutans* biofilm grown with 37.5 mM sucrose.

grown in sucrose-free media form shorter chains of bacterial cells than those with higher concentrations of sucrose and also contain very little EPS. Regions of EPS are observed in only 35% of the top-down images of sucrose-free biofilms, and, where present, are sparse, disconnected, and less than 5 μm in length. When observed with electron microscopy, small clusters of bacteria are seen on the substrates, though the cells do not completely cover the titanium surface, which can be seen underneath the cells (Fig. 3(a)). The incomplete coverage seen in the SEM images of 0 mM sucrose biofilms agrees with the optical images of the biofilms grown with the same concentration in Fig. 2.

In contrast to the sucrose-free biofilm, a biofilm grown with 75 mM sucrose has a more prolific biofilm which covers the titanium surface of the substrate. More bacteria are present in the biofilm samples grown with sucrose, and the bacteria form longer chains of cells relative to the biofilms without sucrose. Biofilms with sucrose also show more EPS surrounding the cells relative to biofilms without sucrose (Fig. 3(b)). EPS in biofilms grown with sucrose is plentiful and continuous across the imaged regions, rather than forming small distinct regions as in the biofilms without sucrose. Bacteria chains and the regions of varied coverage are also seen in previously published electron microscopy images of *S. mutans* biofilms [50,51], though these studies focus on imaging techniques and substrate characteristics rather than the effect of nutrient concentration.

Biofilms grown with 0 mM sucrose (Fig. 4(a)) have fewer cells and less EPS than biofilms grown with sucrose. Biofilms grown with the median sucrose concentrations (37.5, 75, and 375 mM sucrose) have more complete *S. mutans* coverage, as visible in Fig. 4(b), (c), and (d). The biofilms in these images are thicker than the biofilms without

sucrose and show cells that have formed chains with abundant EPS. All biofilms at the median concentrations have complete substrate coverage and no differences are observed for biofilm structure, biofilm quantity, or EPS formation. Though the concentration of sucrose differs across an order of magnitude for these biofilms, visual observation is insufficient to determine the effect of sucrose on biofilm formation. Biofilm presence in these images indicates that the viable sucrose concentration for biofilm growth has a wide range.

At 750 mM sucrose, the biofilms have longer chains and increased surface coverage relative to the biofilms without sucrose but have fewer cells and less EPS compared to biofilms grown with lesser concentrations of sucrose. In Fig. 4(e), the titanium substrate can be seen underneath the 750 mM sucrose biofilm. Cai *et al.* demonstrate the effects of sucrose concentration on the volume of EPS in *S. mutans* biofilms [17,19]. Biofilms in these studies that are grown without sucrose show no EPS. The authors also show that thickness of the biofilms and volume of the EPS initially increases with increasing sucrose, followed by a decrease in the thickness of the biofilm and the quantity of EPS above a certain concentration of sucrose, results that correlate with the results of the electron microscopy imaging presented here.

ImageJ is used to determine the percentage of the field of view that is covered by biofilm for each sucrose concentration. Three representative SEM images at 2500x are chosen for surface coverage analysis for each sucrose concentration and are reported in Table 1. Fig. 5 shows the average field of view concentration for each sucrose concentration with error bars that correspond to one standard deviation of the set of three measurements. Biofilms grown with 0 mM sucrose have an average coverage of $15.7 \pm 4.8\%$, which is significantly lower than any of the

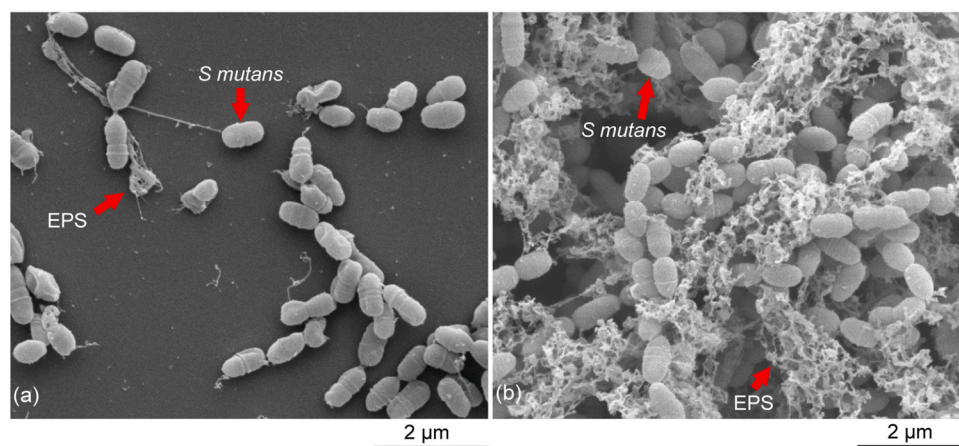


Fig. 3. SEM images of *S. mutans* biofilms at 15000x magnification grown in THY on a titanium-coated substrate with (a) 0 mM sucrose (b) 75 mM sucrose.

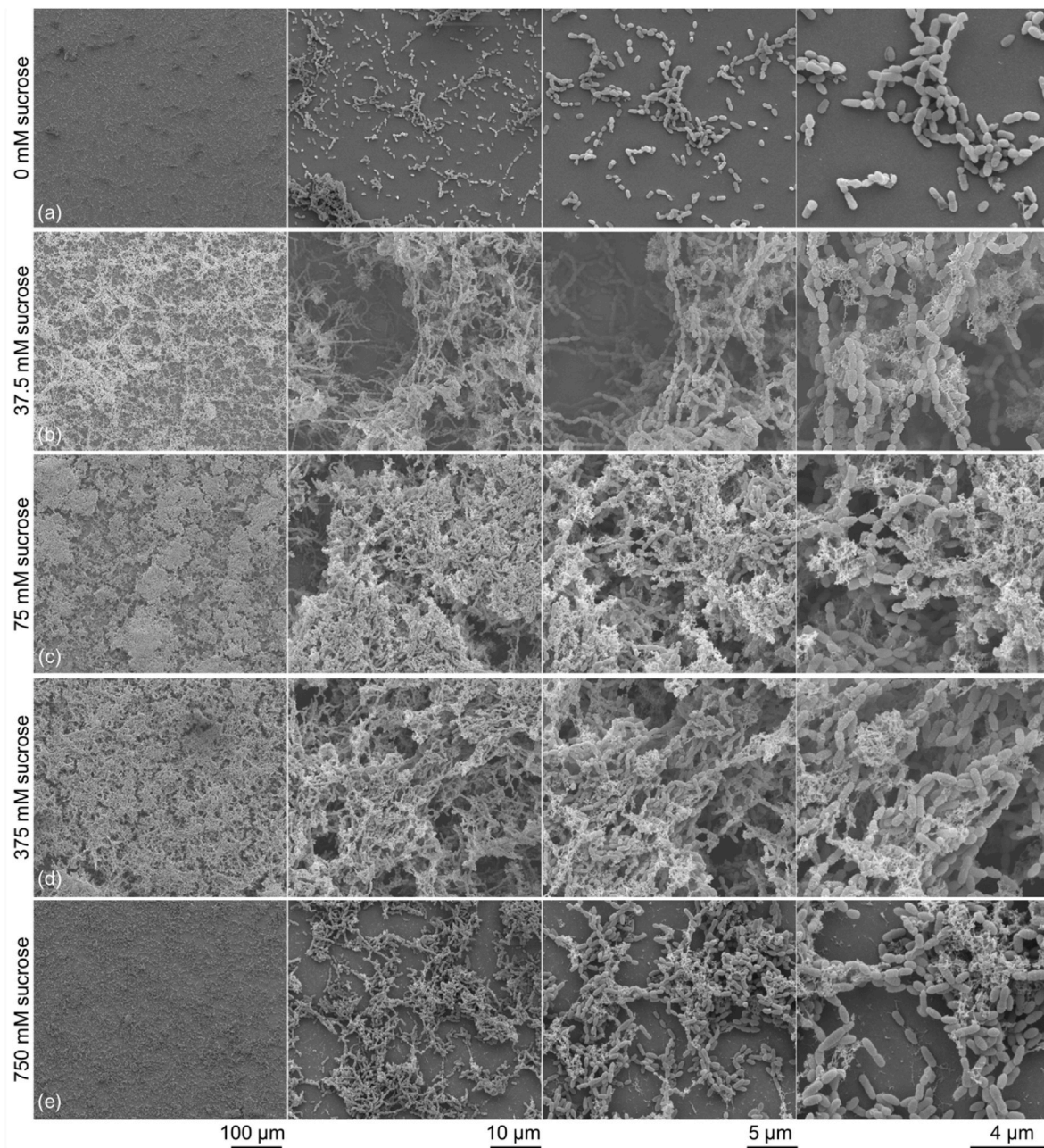


Fig. 4. SEM images of *S. mutans* biofilms grown on titanium coated substrates with increasing concentrations of sucrose by row and increasing magnification (Left to Right: 250x, 2500x, 5000x, 10000x) (a) 0 mM sucrose (b) 37.5 mM sucrose (c) 75 mM sucrose (d) 375 mM sucrose (e) 750 mM.

biofilms grown with sucrose. The low quantitative area coverage corresponds to the incomplete film coverage seen in the optical images in Fig. 2.

Biofilms grown with sucrose all have average coverages above 88%. Biofilms grown with 37.5 mM sucrose have an average coverage of $88.8 \pm 8.0\%$. Biofilms grown with 75 mM sucrose have the highest coverage of $97.6 \pm 2.1\%$. Biofilms with the highest sucrose concentrations, 375 and 750 mM, have average coverages of $93.2 \pm 7.7\%$ and $90.5 \pm 3.8\%$, respectively.

3.3. Electron microscopy profile imaging

Top-down SEM imaging of *S. mutans* biofilms [42,50,52,53] and biofilms of other species [54,55] exists in the literature, and while this technique is useful for determining biofilm coverage and presence, top-down imaging cannot provide information about the height and

formation of elevated features in the biofilm.

Electron microscopy imaging of biofilm profiles reveals details about the structure and formation of biofilms for each sucrose concentration at high magnifications. The electron microscope is focused first on the edge of the substrate and then subsequently farther away to image elevated structures within the biofilms. Fig. 6 demonstrates the imaging process on a biofilm with 37.5 mM sucrose. The long depth of focus and variable working distance of an electron microscope enables imaging of complex biofilm features away from the edge of the substrate.

SEM profile imaging reveals that biofilms do not have a consistent profile or thickness at this scale, but instead have intermittent elevated features with complex geometries. These elevated features could be seen in top-down imaging, but specific details of the features are more easily seen in profile imaging. The elevated features are often delicate, as seen in Figs. 6 and 7, and consist of both bacterial cells and EPS. Images from a biofilm grown with 37.5 mM sucrose show a large cluster of cells

Table 1

Average \pm standard deviation biofilm thickness and average \pm standard deviation height of elevated biofilm features from side-profile SEM images ranging from 496x to 6006x magnification, and average \pm standard deviation percentage of field of view that is covered by biofilms in top-down SEM images at 2500x magnification for each sucrose concentration. Significance testing performed by one-way Anova, significant at $p < 0.05$. Superscript letters are a = significant vs 0 mM, b = significant vs 37.5 mM, c = significant vs 75 mM, d = significant vs 375 mM, e = significant vs 750 mM. P-values and raw data are included in data availability statement.

Sucrose (mM)	Biofilm Thickness (μm)	n =	Elevated Features (μm)	n =	Biofilm Coverage (%)	n =
0	0.3 ± 0.005 ^{b,d,e}	3	2.5 ± 1.1 ^{b,c,d,e}	7	15.7 ± 4.8 ^{b,c,d,e}	3
37.5	4.4 ± 0.35 ^a	3	10.8 ± 10.0 ^a	5	88.8 ± 8.01 ^a	3
75	23.0 ± 14	4	21.5 ± 28.6 ^{a,e}	4	97.7 ± 2.1 ^{a,e}	3
375	16.8 ± 5.5 ^a	3	46.5 ± 41.4 ^{a,e}	4	93.2 ± 7.7 ^a	3
750	20.2 ± 3.5 ^a	4	12.2 ± 3.4 ^{a,c,d}	3	90.5 ± 3.8 ^{a,c}	3

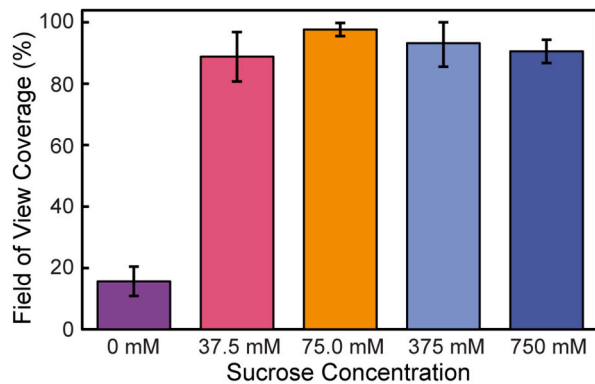


Fig. 5. Percent of field of view that is covered by biofilms in top-down SEM images at 2500x magnification. Error bars represent the standard deviation from three representative measurements.

cantilevered from a narrow support only a few cells across (Fig. 7(a)) and a single chain of cells which extends vertically surrounded by EPS (Fig. 7(b)). The elevated features in focus in these images are located away from the edge of the substrate and rise above the cells in the foreground of the images. Detailed images of the formation of these biofilms, which cannot be discerned with top-down SEM imaging, demonstrate the effectiveness of both the fixation method and the SEM technique for imaging biofilm formation.

In contrast, biofilms grown without sucrose do not exhibit the biofilm thickness or the complex features seen in all biofilms grown with sucrose in this study. Profile imaging shows that the biofilm, where present, is commonly only a single cell in thickness. Small, sparse mounds that are clusters of cells greater than one cell in thickness are seen in 83% of locations imaged on sucrose-free biofilms during this study. All imaged mounds in sucrose-free biofilms are less than 10 μm tall, as seen in Fig. 8. Profile images of the 0 mM sucrose biofilms agree with both optical and top-down SEM images of biofilms in this study, which show that biofilms grown without sucrose have much less substrate coverage than those grown with sucrose.

ImageJ is used to measure the thickness of the biofilm and the elevated biofilm features that rise above the normal biofilm level. Thickness measurements are presented in Fig. 9 with solid bars representing the average biofilm thickness at three locations for each concentration. In the same figure, striped bars are used to represent the average height of elevated features above normal biofilm thickness. Error bars on the biofilm height measurements represent the standard deviation of 3–7 measurements of elevated features, depending on the quantity of elevated features present in the field of view. Biofilm thickness measurements and elevated feature measurements appear in Table 1.

Biofilms grown without sucrose have an average thickness of $0.34 \pm 0.005 \mu\text{m}$, as the biofilm often consists of only one cell or no cells in each image. All biofilms grown with sucrose have sufficient coverage such that the substrates could not consistently be seen in profile imaging. Biofilms grown with 37.5 mM sucrose have an average thickness of 4.4

$\pm 0.35 \mu\text{m}$, which is thicker than biofilms without sucrose but still less than all other sucrose-fed biofilms. The biofilms with 75 mM sucrose have the highest normal average thickness of $23.0 \pm 14.0 \mu\text{m}$, which agrees with the highest area coverage results for the same concentration. Higher sucrose concentrations, 375 and 750 mM have heights of $16.8 \pm 5.5 \mu\text{m}$ and $20.2 \pm 3.5 \mu\text{m}$, respectively. The increased biofilm thickness seen in the biofilms grown with sucrose agrees with previous studies using confocal microscopy that show increased thickness of biofilms with sucrose relative to biofilms grown in media without sucrose [16].

Biofilms grown with sucrose also have mounds of bacteria and EPS that are distinct and elevated above the more consistent lower regions of the biofilm. The heights of these elevated features are shown in Fig. 9 and are represented by striped bars. Biofilms without sucrose have occasional elevated features which consist of cells without EPS, which have an average height of $2.5 \pm 1.1 \mu\text{m}$. When the concentration of sucrose is increased to 37.5 mM, the elevated features begin to consist of elevated cells with EPS and have an average height of $10.8 \pm 10.0 \mu\text{m}$. Biofilms with 75 and 375 mM sucrose have the tallest average feature heights of $21.5 \pm 28.6 \mu\text{m}$ and $46.5 \pm 41.4 \mu\text{m}$, respectively. These heights agree with the biofilm coverage results discussed previously, in which 75 and 375 mM concentrations also exhibited large field of view coverage in top down SEM imaging. As the sucrose concentration increases from 375 mM to 750 mM sucrose, the average height of the elevated features decreases to $12.2 \pm 3.4 \mu\text{m}$. Biofilms with 75 and 375 mM sucrose each have multiple mounds above 100 μm in height, but the maximum feature height for 37.5 or 750 mM biofilms is less than 50 μm . Elevated mounds in biofilms with 75 and 375 mM sucrose are shown in Fig. 10. The presence of large mounds in biofilms grown with both 75 and 375 mM sucrose indicates a large range of sucrose concentrations is viable for biofilm growth. In a previous study of biofilm formation using confocal laser scanning microscopy, Cai *et al.* described the presence of similar bacterial mounds in *S. mutans* biofilms, as well as increased quantities of EPS in biofilms between 30 and 300 mM sucrose relative to biofilms with 0 or 1100 mM sucrose [17].

Hollow areas at the base of elevated mounds are visible when the bases were not blocked by other features. Bacterial biofilms form in “microcolonies” consisting of bacteria, EPS, and channels for fluid transport [12,56]. Hollow features noted in Fig. 10 could be these channels, and similar features are reported in other studies using top-down SEM imaging [50].

3.4. Laser spallation

Weibull modeling of film failure is shown in Fig. 11. Alpha and beta, the Weibull parameters used to produce the curves in Fig. 11, and the adhesion strength values for each sucrose concentration are included in Table 2. Adhesion results indicate that sucrose plays a key role in the adhesion strength of *S. mutans* biofilms and that these biofilms are tolerant of a wide range of sucrose concentrations. The relationship between sucrose concentration and adhesion strength suggests a concentration around 75 mM that maximizes the adhesion of *S. mutans* biofilms to titanium.

For biofilms grown with 0 mM sucrose, the measured adhesion

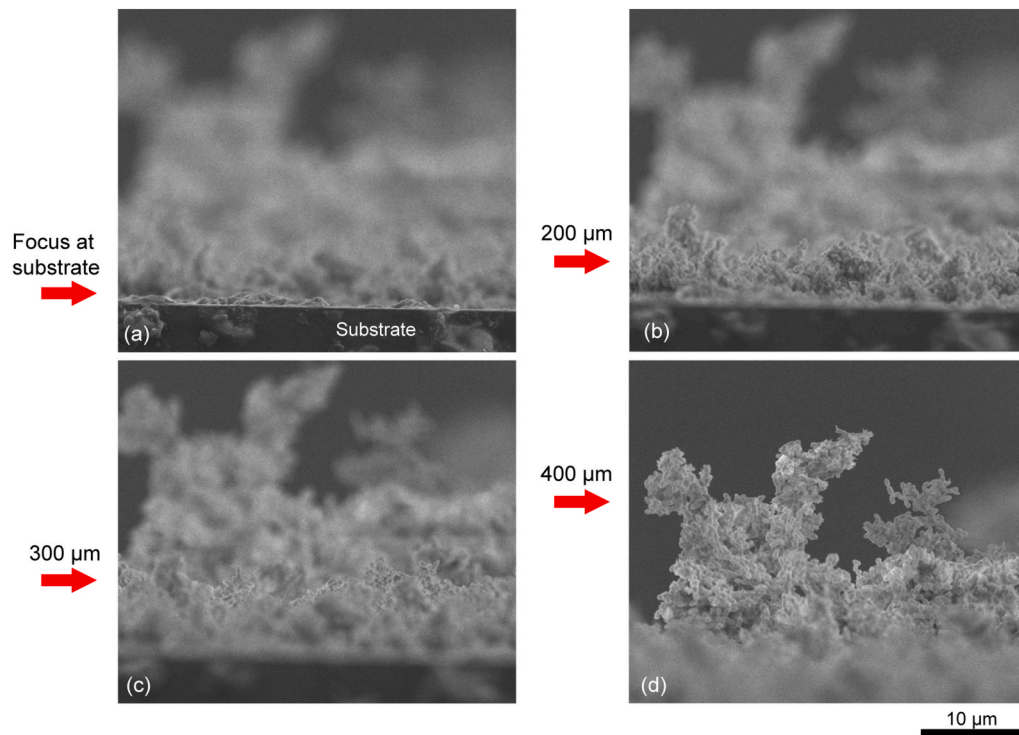


Fig. 6. Profile SEM images of *S. mutans* biofilm with 37.5 mM sucrose on titanium coated substrates with arrows noting focused region at (a) edge of substrate (b) 200 μm from edge of substrate (c) 300 μm from edge of substrate (d) 400 μm from edge of substrate.

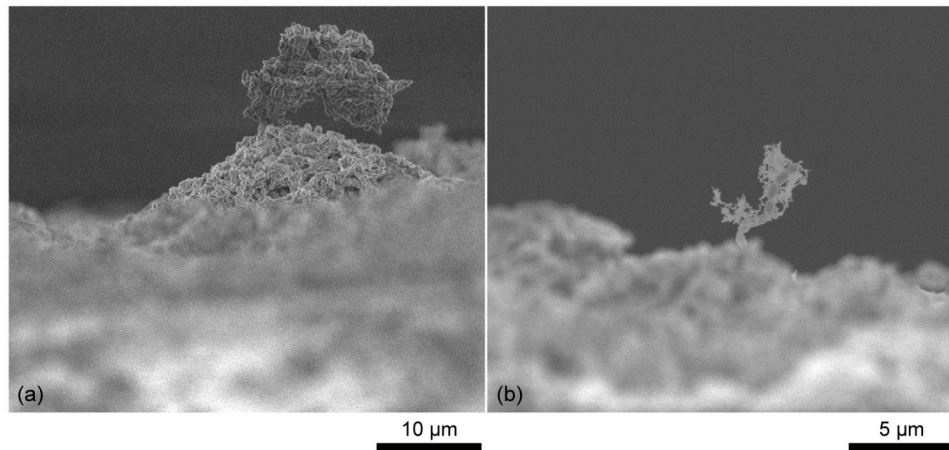


Fig. 7. SEM images of structures in a *S. mutans* biofilm grown with 37.5 mM sucrose demonstrating that the microscopy preparation technique preserves (a) the formation of bacteria cells and (b) EPS formation.

strength is 89.1 MPa with a 95% CI (77.8, 100.4). The adhesion strength increases for biofilms grown with 37.5 mM sucrose which have a measured adhesion strength of 167.3 MPa with 95% CI (157.0, 178.3). Biofilms grown with 75 mM sucrose exhibit the maximum measured adhesion strength of tested concentrations at 336 MPa with a 95% CI (329.5, 342.5). Above 75 mM sucrose, the measured adhesion strength decreases with increasing sucrose concentration. Biofilms grown with 375 mM sucrose exhibit a measured adhesion strength of 301.5 MPa with 95% CI (291.9, 311.5). Biofilms with 750 mM sucrose, the maximum concentration tested in this study, exhibit a measured adhesion strength of 262.9 MPa and a 95% CI (247.8, 278.0). The results of the adhesion study agree with biofilm coverage and biofilm thickness

measurements. Biofilms grown without sucrose exhibit significantly lower coverage and lower adhesion strength compared to biofilms with sucrose. The laser spallation technique applies the shock load uniformly across the rear side of the substrate in the loading area, which is a circle with a diameter of 2 mm. Therefore, even though the biofilm coverage is uneven in the loading region, the load is still applied to the macroscale biofilm that is present within 2 mm whereas our coverage measurements from SEM image analysis are a field of view of $56 \times 56 \mu\text{m}$.

These results demonstrate the success of the laser spallation technique in determining the adhesion characteristics of heterogeneous materials like biofilms, which are loosely cohesive and consist of non-uniform structures. The laser spallation technique, which applies the

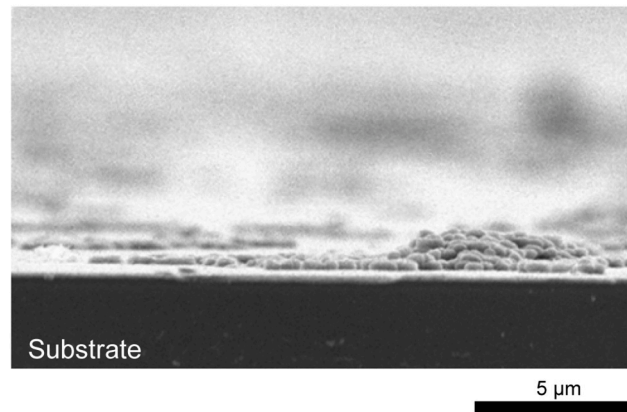


Fig. 8. SEM profile image of *S. mutans* biofilm grown on a titanium-coated substrate with 0 mM sucrose.

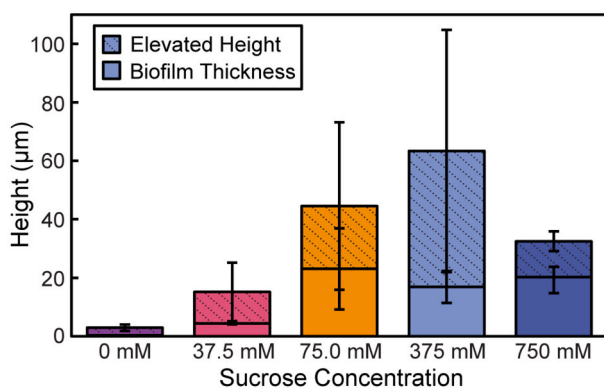


Fig. 9. Thickness measurements of biofilms (solid bars) and elevated biofilm features (striped bars) from side-profile SEM images for each sucrose concentration. Error bars represent one standard deviation of 3–7 measurements for each concentration.

loading force uniformly across the substrate in the loading area, can be used to determine consistent results with narrow confidence intervals. Because the effect of sucrose on biofilm adhesion is non linear, but changes direction at a turning point concentration, a characterization method which can provide consistent results for heterogeneous

materials is a necessity. The laser spallation technique can then be used to characterize the effect of other growth conditions, such as media viscosity or flow conditions, on the adhesion properties of biofilms.

While a statistical decrease in adhesion strength is seen for sucrose concentrations above 75 mM, the decrease is not large relative to the increase in sucrose concentration. Between 75 mM and 750 mM sucrose, the decrease in adhesion strength is 22% while the sucrose concentration increases by an order of magnitude. Adhesion strength results support the trend seen in this work that a wide range of sucrose concentrations exists that is viable for biofilm growth. Differences in biofilm characteristics for individual sucrose concentrations are small relative to the change in magnitude in sucrose concentration, a trend which has been seen in other studies quantifying the amount of EPS in *S. mutans* biofilms [17]. The mechanism by which sucrose restricts biofilm adhesion at high concentrations is not yet well understood, though some previous studies propose that the increased osmotic pressure of the media may contribute to the reduction in biofilm growth and EPS formation [18].

Adhesion strength values of all *S. mutans* biofilms in this study are shown in Fig. 12 and compared to measured adhesion strength of osteoblast-like cells from Boyd et al. [30]. Boyd et al. used the laser spallation technique to measure the adhesion strength of MG63 osteosarcoma cells to titanium coated substrates and found their adhesion strength to be 143 MPa with 95% CI (114, 176) [30]. Without sucrose, the measured adhesion strength of *S. mutans* biofilms is less than that of the osteoblast-mimicking cells, so the body may have a better chance to

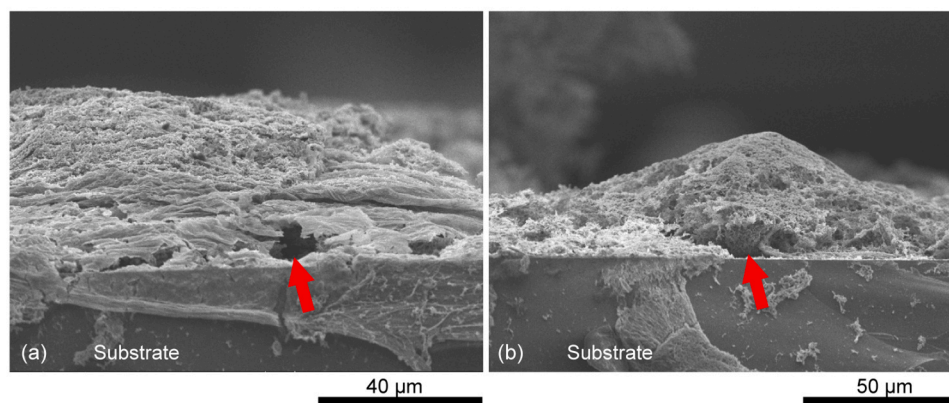


Fig. 10. SEM images of channels inside thick regions of *S. mutans* biofilm grown with (a) 75 mM sucrose (b) 375 mM sucrose. Multiple channel-like regions are visible at the base of the biofilm mounds, one of which is indicated by the arrow.

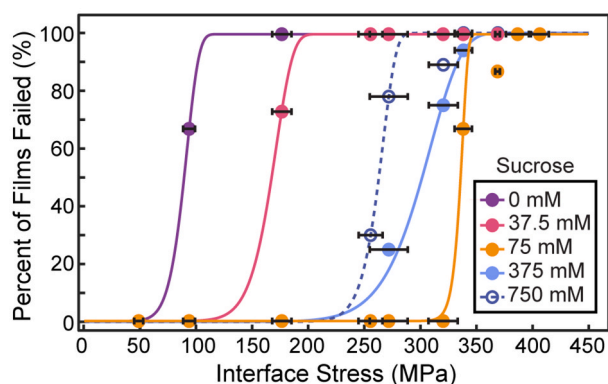


Fig. 11. Percent of biofilms failed at increasing interface stress. Data points represent experimental data. Lines represent Weibull fitting of experimental data. Biofilms cultured with sucrose concentrations of 0–75 mM exhibit an increase in interface stress needed to initiate film failure with increasing sucrose concentration. Biofilms cultured with sucrose concentrations greater than 75 mM, i.e., 375 mM and 750 mM, exhibit a decrease in interface stress needed to initiate film failure with increasing sucrose concentration. Horizontal error bars are the standard deviation of the calibrated interface stress at each point.

Table 2

Adhesion strength for each sucrose concentration, corresponding Weibull parameters, and root mean square (RMS) difference between Weibull model and experimental data. Percentile bootstrap estimates are used to produce the 95% confidence intervals listed in parenthesis. *There is no difference between model fit and experimental data.

Sucrose (mM)	Adhesion Strength (MPa)	α Parameter	β Parameter	RMS
0	89.1 (77.8, 100.4)	92.7 (80.6, 104.8)	9.38 (2.9, 29.9)	0.0000*
37.5	167.3 (157.0, 178.3)	172.4 (163.2, 182.1)	12.2 (4.3, 34.6)	0.0000*
75	336 (329.5, 342.5)	337.9 (329.8, 346.0)	66.6 (35.6, 124.5)	0.0433
375	301.5 (291.9, 311.5)	310.9 (300.5, 321.7)	12.0 (3.7, 39.0)	0.0383
750	262.9 (247.8, 278.0)	267.1 (251.5, 282.7)	23.53 (11.8, 46.8)	0.367

resolve *S. mutans* colonies. However, in the presence of 37.5 mM sucrose, the lowest sucrose concentration tested in this work, and the higher sucrose concentrations included in this study, the adhesion strength of *S. mutans* biofilms becomes stronger than the adhesion strength of MG 63 cells to the same substrate. The effect of sucrose on the adhesion of MG63 cells to titanium surfaces is currently unknown, though glucose is a nutrient commonly used in culturing MG63 cells. Determining the effect of the nutrient concentration on the adhesion of MG63 cells is an area of future study.

The range of sucrose concentrations in this work is relevant to common food items that increase sucrose in the environment surrounding a dental implant during consumption. A previous study by Dawes et al. [23] determined that the concentration of sucrose in saliva after 10 min of gum chewing is approximately 30 mM. A commercial soy milk has a sucrose concentration of approximately 73 mM [57], similar to the sucrose concentration associated with the maximum biofilm adhesion strength found in this work. Lemon-lime Gatorade has a sucrose concentration of 170 mM [58]. Coca-Cola has a sucrose concentration of approximately 320 mM [59]. Other common foods have still higher sucrose concentrations, such as a commercial fruit jam which has a sucrose concentration of over 2 M [60].

Diets high in sugar are known to contribute to the risk of the development of dental caries [61]. Initial studies into the relationship between sugar and peri-implantitis show that sugar consumption has a plaque-promoting effect at implant sites as well as an association with peri-implant mucositis and peri-implantitis [62]. Experimental animal studies have also used processed, high-carbohydrate diets to provoke corresponding peri-implant inflammation [63]. Sucrose present in the implant environment that contributes to prolific biofilm growth and increased biofilm adhesion to the implant surface likely increases the risk of developing peri-implantitis as well.

4. Conclusions

Robust and adherent biofilm colonization on an implant surface can lead to infection. The environment surrounding dental implants including substrate material and nutrient concentration, affect the propensity for biofilm growth and thus may alter the likelihood for infections to occur. In this work, the adhesion and formation of *S. mutans* biofilms on titanium substrates are studied in the presence of varying sucrose concentration from 0 mM to 750 mM. Adhesion strength values for biofilms are compared to those of osteoblast-mimicking cells to determine if sucrose presence may help biofilms to outcompete osteoblasts during osseointegration of dental implants. Biofilms grown with 0 mM sucrose form much shorter chains and much less EPS than biofilms grown with sucrose, and the sporadic substrate coverage can be seen optically. In biofilms grown with sucrose, elevated mounds and fragile features comprised of cells and EPS are preserved and imaged with electron microscopy. The highest elevated mounds are seen in biofilms grown with 75 and 375 mM sucrose and exhibit transport channels as reported in other work. A wide range of sucrose concentrations resulted in plentiful formation and adhesion of *S. mutans* biofilms on implant surfaces.

The laser spallation method is used to quantitatively determine the adhesion strength of the biofilms to titanium substrates. Maximum adhesion strength occurs in biofilms grown with 75 mM sucrose. For sucrose concentrations above 75 mM, the adhesion strength decreases, and biofilms grown with 750 mM sucrose have an adhesion strength that is 22% lower than 75 mM sucrose. The decrease in adhesion strength is small relative to the increase in sucrose, which agrees with trends seen in electron microscopy images of the same biofilms. The least adherent biofilms are produced by the growth condition without sucrose and have an adhesion strength that is 73% lower than the 75 mM sucrose condition. Sucrose enhances the EPS production of *S. mutans* biofilms and increases the adhesion strength to titanium. Adhesion strength of *S. mutans* biofilms with sucrose to titanium is greater than the adhesion

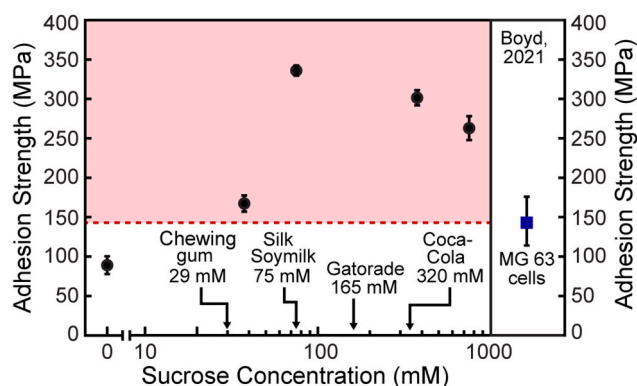


Fig. 12. Black circles represent *S. mutans* biofilm adhesion strength to titanium substrates for each sucrose concentration. The blue square and dashed red line show adhesion strength of MG 63 cells to the same substrates as previously determined by Boyd et al. [30]. Error bars are the 95% CI determined by percentile bootstrap estimates. Sucrose concentrations of common commercial food products are noted [23,57–59]. (For interpretation of the references to colour in this figure legend, the reader is referred to the Web version of this article.)

strength of osteoblast-like cells to the same surface, which suggests that sugary foods may help *S. mutans* biofilms outcompete osteoblasts during osseointegration. Sugar-rich diets are a well-known risk factor for dental caries and are also associated with peri-implantitis. Sucrose-mediated biofilm adhesion and formation on titanium is a possible mechanism to explain how sucrose in the environment could lead to higher rates of peri-implantitis.

Funding

This material is based upon work supported by the National Science Foundation CAREER Award grant number 2045853 and National Aeronautics and Space Administration grant number 80NSSC20M0251. We gratefully acknowledge NIH funding under grant numbers P20GM130456, P20GM103436 and R03DE029547 for completion of these experiments. This work is also made possible by the University of Kentucky University Research Postdoctoral Fellowship (L.W.), as well as the University of Kentucky College of Engineering through the Engineering Summer Undergraduate Research Fellowship (T.B.). Any opinions, findings, and conclusions or recommendations expressed in this material are those of the authors and do not necessarily reflect the views of the National Science Foundation.

Declaration of interests

The authors declare the following financial interests/personal relationships which may be considered as potential competing interests: Martha Grady reports financial support was provided by National Institutes of Health. Martha Grady reports financial support was provided by National Science Foundation. Martha Grady reports financial support was provided by National Aeronautics and Space Administration.

CRediT authorship contribution statement

Laura J. Waldman: Methodology, Formal analysis, Investigation, Data curation, Supervision, Writing – original draft, Writing – review & editing. **Tony Butera:** Methodology, Formal analysis, Data curation, Writing – original draft, Writing – review & editing. **James D. Boyd:** Investigation, Data curation, Methodology, Supervision. **Martha E. Grady:** Supervision, Funding acquisition, Conceptualization, Investigation, Project administration, Resources, Visualization, Writing – review & editing.

Data availability

We have published our data and it is freely available via a link <https://doi.org/10.18126/d1bg-nwtg> from the Materials Data Facility.

Acknowledgments

Scanning electron microscopy was performed in the Electron Microscopy Center at the University of Kentucky, and the authors wish to thank Nicolas Briot for assistance with specimen preparation. The authors wish to thank Natalia Korotkova for the generous donation of *S. mutans* Xc and Arnold Stromberg with the Applied Statistics Laboratory for the Weibull modeling and analysis. The authors also wish to thank Dr. Craig Miller and Dr. David DeVito for their guidance, as well as Svetlana Zamakhaeva for the CFU assay. Atomic force microscopy was performed in the Light Microscopy Core at the University of Kentucky.

References

- [1] Huang H-L, et al. Antibacterial TaN-Ag coatings on titanium dental implants. *Surf Coating Technol* 2010;205(5):1636–41.
- [2] Albrektsson T, Johansson C. Osteoinduction, osteoconduction and osseointegration. *Eur Spine J* 2001;10(2):S96–101.

- [3] Pye AD, et al. A review of dental implants and infection. *J Hosp Infect* 2009;72(2):104–10.
- [4] Sakka S, Baroudi K, Nassani MZ. Factors associated with early and late failure of dental implants. *Journal of Investigative and Clinical Dentistry* 2012;3(4):258–61.
- [5] Costerton JW, Montanaro L, Arciola CR. Biofilm in implant infections: its production and regulation. *Int J Artif Organs* 2005;28(11):1062–8.
- [6] Wu H, et al. Strategies for combating bacterial biofilm infections. *Int J Oral Sci* 2015;7(July):1–7.
- [7] Mongkolroob R, Taweechaisupapong S, Tungpradabkul S. Correlation between biofilm production, antibiotic susceptibility and exopolysaccharide composition in *Burkholderia pseudomallei* bpsI, ppk, and rpoS mutant strains. *Microbiol Immunol* 2015;59(11):653–63.
- [8] Karygianni L, et al. Biofilm matrixome: extracellular components in structured microbial communities. *Trends Microbiol* 2020;28(8):668–81.
- [9] Nandakumar V, et al. Characteristics of bacterial biofilm associated with implant material in clinical practice. *Polym J* 2013;45(2):137–52.
- [10] Boudarel H, et al. Towards standardized mechanical characterization of microbial biofilms: analysis and critical review. *npj Biofilms and Microbiomes* 2018;4(1).
- [11] Mei L, Busscher HJa. Influence of surface roughness on streptococcal adhesion forces to composite resins. *Dent Mater* 2011;27(8):770–8.
- [12] Kishen A, Haapasalo M. Biofilm models and methods of biofilm assessment. *Endod Top* 2012;22:58–78.
- [13] Saeki D, et al. Effect of hydrophobicity of polymer materials used for water purification membranes on biofilm formation dynamics. *Colloids Surf A Physicochem Eng Asp* 2016;506:622–8.
- [14] Loo CY, Corliss DA, Ganeshkumar N. *Streptococcus gordonii* biofilm formation: identification of genes that code for biofilm phenotypes. *J Bacteriol* 2000;182(5):1374–82.
- [15] Stoodley P, et al. Influence of hydrodynamics and nutrients on biofilm structure. *J. Appl. Microbiol. Symposium Supplement* 1999;85(28):19–28.
- [16] Shemesh M, Tam A, Steinberg D. Expression of biofilm associated genes of *Streptococcus mutans* in response to glucose and sucrose. *J Med Microbiol* 2007;56:1528–35.
- [17] Cai JN, et al. Functional relationship between sucrose and a cariogenic biofilm formation. *PLoS One* 2016;11(6):1–12.
- [18] Boyd JD, Korotkova N, Grady ME. Adhesion of biofilms on titanium measured by laser-induced spallation. *Exp Mech* 2019;59(9):1275–84.
- [19] Cai JN, et al. Sucrose challenges to *Streptococcus mutans* biofilms and the curve fitting for the biofilm changes. *FEMS (Fed Eur Microbiol Soc) Microbiol Ecol* 2018;94(7):1–9.
- [20] Liu R, et al. Antibacterial effect of copper-bearing titanium alloy (Ti-Cu) against *Streptococcus mutans* and *Porphyromonas gingivalis*. *Sci Rep* 2016;6(June):1–10.
- [21] Grner-Schreiber B, et al. Plaque formation on surface modified dental implants. 2001. p. 543–51.
- [22] Souza JCM, et al. Corrosion behaviour of titanium in the presence of *Streptococcus mutans*. *J Dent* 2013;41(6):528–34.
- [23] Dawes C, et al. The distribution of saliva and sucrose around the mouth during the use of chewing gum and the implications for the site-specificity of caries and calculus deposition. *J Dent Res* 1993;72(5):852–7.
- [24] Leme AFP, et al. The role of sucrose in cariogenic dental biofilm formation - new insight. *J Dent Res* 2006;85(10):878–87.
- [25] Wang C, et al. Emergent properties in *Streptococcus mutans* biofilms are controlled through adhesion force sensing by initial colonizers. *mBio* 2019;10(5).
- [26] Wang C, et al. *Streptococcus mutans* adhesion force sensing in multi-species oral biofilms. *npj Biofilms and Microbiomes* 2020;6(1):25.
- [27] Prades L, et al. Computational and experimental investigation of biofilm disruption dynamics induced by high-velocity gas jet impingement. *mBio* 2020;11(1).
- [28] Busscher HJa. Microbial adhesion in flow displacement systems. *Clin Microbiol Rev* 2006;19(1):127–41.
- [29] Gomes LC, Mergulho FJ. SEM analysis of surface impact on biofilm antibiotic treatment. *Scanning* 2017;2017(c).
- [30] Boyd JD, et al. Biofilm and cell adhesion strength on dental implant surfaces via the laser spallation technique. *Dent Mater* 2021;37(1):48–59.
- [31] Ehsani H, et al. Evolution of the laser-induced spallation technique in film adhesion measurement. *Appl Mech Rev* 2021;73(3).
- [32] Paltauf G, Schmidt-Kloiber H. Microcavity dynamics during laser-induced spallation of liquids and gels. *Applied Physics A: Materials Science & Processing* 1996;62(4):303–11.
- [33] Tanaka K, et al. Engineering the interface: effects of interfacial adhesion and substrate thickness on the ductility of polymer-supported metal films. *Experimental Mechanics* 2022;62(1):49–58.
- [34] Kuznetsov AI, et al. Laser-induced jet formation and droplet ejection from thin metal films. *Applied Physics A: Materials Science and Processing* 2012;106(3):479–87.
- [35] Kandula SSV, et al. Dynamic delamination of patterned thin films. *Applied Physics Letters* 2008;93(26).
- [36] Jajam KC, Sottos NR. Energy absorption behavior of polyurea under laser-induced dynamic mixed-mode loading. *Journal of Dynamic Behavior of Materials* 2016;2(3):379–90.
- [37] Hu L, et al. Cell adhesion measurement by laser-induced stress waves. *Journal of Applied Physics* 2006;100(8).
- [38] Youssef G, Gupta V. Dynamic tensile strength of polyurea. *Journal of Materials Research* 2012;27(2):494–9.
- [39] Huynh NU, Gamez C, Youssef G. Spectro-Microscopic characterization of elastomers subjected to laser-induced shock waves. *Macromolecular Materials and Engineering* 2022;307(2):1–14.

- [40] Grady ME, et al. Shockwave loading of mechanochemically active polymer coatings. *ACS Applied Materials and Interfaces* 2014;6(8):5350–5.
- [41] Hagerman E, et al. Evaluation of laser spallation as a technique for measurement of cell adhesion strength. *Journal of Biomedical Materials Research Part A* 2007;82A(4):852–60.
- [42] Relucanti M, et al. Microscopy methods for biofilm imaging: focus on sem and VP-SEM pros and cons. *Biology* 2021;10(1):1–17.
- [43] Edgar RJ, et al. Discovery of glycerol phosphate modification on streptococcal rhamnase polysaccharides. *Nat Chem Biol* 2019;15(5):463–71.
- [44] Dassanayake RP, et al. Identification of a reliable fixative solution to preserve the complex architecture of bacterial biofilms for scanning electron microscopy evaluation. *PLoS ONE* 2020;15(5):1–15.
- [45] Blaiszik BJ, et al. The materials data facility: data services to advance materials science Research. *Jom* 2016;68:2045–52.
- [46] Blaiszik BJ, et al. A data ecosystem to support machine learning in materials science. *MRS Communications* 2019:1–9.
- [47] Murthy DP, Xie M, Jiang R. Weibull models, vol. 505. John Wiley & Sons; 2004.
- [48] van der Mei HC, de Vries J, Busscher HJ. Weibull analyses of bacterial interaction forces measured using AFM. *Colloids Surf B: Biointerfaces* 2010;78(2):372–5.
- [49] Mei L, et al. Influence of surface roughness on streptococcal adhesion forces to composite resins. *Dent Mater* 2011;27(8):770–8.
- [50] Weber K, et al. Comparison of SEM and VPSEM imaging techniques with respect to *Streptococcus mutans* biofilm topography. *FEMS Microbiology Letters* 2014;350(2):175–9.
- [51] Park JW, et al. The effects of surface roughness of composite resin on biofilm formation of *Streptococcus mutans* in the presence of saliva. 2012. p. 532–9.
- [52] Vyas N, et al. A quantitative method to measure biofilm removal efficiency from complex biomaterial surfaces using SEM and image analysis. *Scientific Reports* 2016;6(August):2–11.
- [53] Asahi Y, et al. Simple observation of *Streptococcus mutans* biofilm by scanning electron microscopy using ionic liquids. *AMB Express* 2015;5(1):0–8.
- [54] Alhede M, et al. Combination of microscopic techniques reveals a comprehensive visual impression of biofilm structure and composition. *FEMS Immunology and Medical Microbiology* 2012;65(2):335–42.
- [55] Boss. Characterization of *scardovia wiggisiae* biofilm by original scanning electron microscopy protocol. *Microorganisms* 2020;8(6):1–16.
- [56] Hall-Stoodley L, Costerton JW, Stoodley P. Bacterial biofilms: from the natural environment to infectious diseases. *Nature Reviews Microbiology* 2004;2(2):95–108.
- [57] Inc. W.S. Original soymilk [cited 2022 2022-07-09]; Available from: <https://silk.com/plant-based-products/soymilk/original-soymilk/>; 2022.
- [58] Inc. S.-V.C. Gatorade thirst quencher [cited 2022 2022-07-09]; Available from: <https://www.gatorade.com/fuel/hydration/gatorade-thirst-quencher/bottle/lemon-lime>; 2022.
- [59] Company TC-C. Coca-cola [cited 2022 2022-07-09]; Available from: <https://us.coca-cola.com/products/coca-cola/original>; 2022.
- [60] Company JMS. Strawberry jam [cited 2022 2022-07-09]; Available from: <https://www.smuckers.com/fruit-spreads/jam/strawberry-jam>; 2022.
- [61] Pitts NB, et al. Dental caries. *Nature Reviews Disease Primers* 2017;3.
- [62] Souza JGS, et al. Effect of sucrose on biofilm formed in situ on titanium material. *Journal of Periodontology* 2019;90:141–8.
- [63] Vilarrasa J, et al. Exploring the relationship among dental caries, nutritional habits, and peri-implantitis. *Journal of Periodontology* 2021;92:1306–16.